Pergamon

Int. J. Heat Mass Transfer. Vol. 38, No. 14, pp. 2611–2621, 1995

0017-9310/95 $9.50+0.00

0017-9310(95)00004-6

Theoretical investigation of transient droplet combustion by considering flame radiation

KEH-CHIN CHANG and JENG-SHIEN SHIEH

Institute of Aeronautics and Astronautics, National Cheng Kung University, Tainan 70101, Taiwan, Republic of China

(*Received* 18 *April* 1994 *and in final form* 18 *November* 1994)

Abstract—For a droplet burning in quiescent air and in a high temperature environment, conduction and radiation are two major heat transfer modes. Soot formation has been observed in many experiments on single-droplet combustion of different fuels. As a result, radiation heat transfer should play a dominant role in the burning process. In addition, most liquid fuels are semi-transparent materials. The collocation method is applied to solve the radiative heat transfer equation in regard to the droplet interior. The results, including different cases of droplet diameter square, ignition delay time, with and without considering radiation heat transfer, are compared with the experimental data. The prediction of the diameter square when radiation heat transfer is considered agrees more with the experimental data than the case without considering radiation heat transfer.

INTRODUCTION

Numerous modeling studies of droplet combustion processes have been reported in past years. Extensive discussions of these research achievements can be found in the excellent review papers of Law [1] and Faeth [2]. It is noted that the thermal radiative effects on droplet combustion were ignored in most of the past works because of the mathematical and physical complexity of research on radiative transfer (Law [1], Faeth [2] and Viskanta and Mengüç [3]). However, some recent research efforts have included thermal radiative effects in their modeling of droplet combustion. Bergeron and Hallett [4] have included radiation in their numerical model to extract reaction rate constants from the measured data using the suspended droplet technique. Saitoh *et al.* [5] included radiative transfer in their droplet combustion model by treating the gas phase as a participating medium while assuming the droplet to be an opaque material. Their numerical investigation showed that when thermal radiation is considered for the case of *n*-heptane, the maximum flame temperature was reduced by at least 25% when compared to that done without considering thermal radiation. Thus, they concluded that thermal radiation should not be ignored in modeling droplet combustion. Lage and Rangel [6, 7] have calculated droplet vaporization by including thermal radiation absorption. The incident radiation is assumed to be spherically symmetric and to have a blackbody spectral intensity distribution, but the gas phase is assumed to be a nonparticipating medium. Simulations using decane droplets with a radius of 25–100 μm, tested with ambient temperatures from 500 to 1800 K, have concluded that under usual spray combustion conditions, there is not enough radiative energy to induce explosive vaporization of mono-component hydrocarbon droplets, and only the total absorptance values are needed for vaporization studies.

Flame radiation is classified as being nonluminous or luminous. In nonluminous flames, carbon dioxide and water vapor are the most prominent constituents at temperatures up to 3000 K. When soot is present, however, the flame becomes luminous. Siegel and Howell [8] indicated that soot, usually produced in the fuel-rich region of the hydrocarbon flames, can often double or triple the radiant energy emanated by the gaseous products alone.

In a gas turbine combustor, as the fuel spray approaches the flame front, the droplets start to evaporate due to heat transfer from the flame. The smaller droplets in the spray have sufficient time to burn completely, and the fuel vapor mixes with the high temperature air and burns as a premixed flame. The larger droplets in the spray may not have enough time to evaporate completely, and thus, burn as individual droplets (droplet combustion). Since the fuel vapor undergoes high temperature pyrolysis before it is oxidized in the flame, there is a high probability for the intermediate formation of soot. Thus, Sjögren [9] argued that droplet combustion was the cause of soot formation in spray combustion. Experimental observations on soot formation caused by droplet combustion were conducted by Kobayasi [10], who investigated single droplet combustion for several kinds of fuels. Soot formation was observed on many fuels, like benzene, nitrobenzene, heavy oil, etc. The observations of Bolt and Saad [11] indicate that for pure hydrocarbon fuels including *n*-heptane and iso-octane, the luminous regions are at the wake of the droplet, while the combustion of multicomponent fuels like kerosene causes the formation of more soot

NOMENCLATURE

C_f	chemical reaction coefficient
C_p	specific heat capacity at constant pressure
c	constant
D	diffusion coefficient
d	diameter of droplet
E_a	activation energy
$F_{\lambda T\to\infty}$	blackbody fractional emissive power
f_v	volume fraction of soot
h_k	enthalpy for species k
I_k	internal energy for species k
$I_{\lambda b}$	blackbody spectral radiation intensity
L	latent heat
$\dot{m}$	evaporation rate
N	total species number
n	refractive index
p	pressure
p_0	reference saturated pressure
Q	heat of combustion
q	heat flux
R_s	droplet radius
R_u	universal gas constant
r	radial ordinate
T	temperature
T_0	reference saturated temperature
t	time
u	radial velocity
W	molecular weight
X	molar concentration
x	flame thickness
Y	mass fraction.

Greek symbols

α	absorption coefficient
α_p	Planck mean absorption coefficient
α'	order of power for concentration
Γ	transmission fraction [%]
ε	radiation emissivity
κ	thermal conductivity, extinction coefficient
λ	wavelength
ν	dynamic viscosity
ρ	density
σ	Stefan–Boltzmann constant
τ	optical thickness
τ_{rr}, $\tau_{\theta\theta}$, $\tau_{\phi\phi}$	shear stresses
ϕ	flammability
ω	single scattering albedo
$\dot{\omega}$	chemical reaction rate.

Subscripts

b	blackbody
F	fuel
g	nonluminous flame
k	species
l	liquid
O	oxidizer
r	radiation
r, θ, ϕ	spherical coordinate
s	droplet surface, luminous flame
∞	surroundings.

Superscripts

c	chemical reaction
n	iteration number.

and carbon particles. The influence of relative velocity between droplets and the air on soot formation has been described in the experiments of Sjögren [9]. Randolph and Law [12], who investigated the dynamic parameters influencing soot formation and destruction in droplet burning, concluded that as long as the soot is enclosed by the flame, it will eventually be oxidized as the flame regresses inward. Thus, near-complete combustion, with or without micro-explosion, should result in very little soot emission. Randolph and Law [12] also reviewed the fundamental studies on soot formation caused by droplet combustion in experiments conducted between 1973 and 1985.

Hara and Kumagai [13], who conducted experiments for free droplet combustion under microgravity, found that soot formation can be clearly seen on the sequential photographs of a burning *n*-heptane droplet. In the early burning period, the soot shell formed is almost spherical, and then the soot begins to make a tail at the point of its shell. In the final stage of burning, the soot shell disappeared, and only the soot tail was observed. Soot formation was not observed throughout the combustion process of the other fuel sample, ethyl alcohol. Jackson *et al.* [14, 15] provided fundamental qualitative understanding of soot dynamics in droplet combustion experiments performed at low gravity. Their experiments covered soot formation and emissions influenced by small convective flows, initial droplet diameters, and mixture compositions.

Based upon the above observations of soot formation, this work will present a theoretical analysis of droplet combustion by considering thermal radiation from the flame. In addition, it is well aware that most liquid fuels are not perfectly transparent materials, and that liquid fuels may emit/absorb part of the radiative heat flux to/from the surrounding environment. Internal radiation absorption is thus considered in this model.

Benzene, a fuel sample frequently used in single droplet combustion experiments, is used as the test fuel in this study because measured data of benzene droplet combustion is readily available, because all

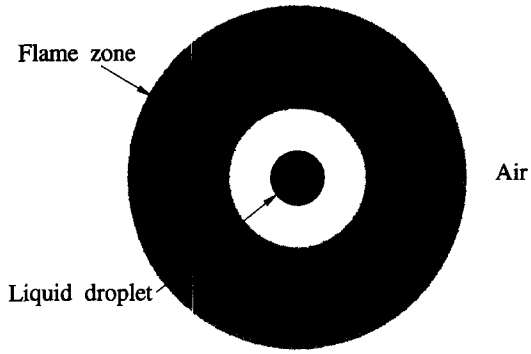

Fig. 1. Schematic view of single droplet combustion.

the physical properties of benzene are easy to find, and because soot formation is observed in benzene droplet combustion.

THEORETICAL FORMULATION

Consider a fuel droplet suddenly exposed to a hot, quiescent air environment. The droplet, heated by conduction flux from the high temperature surroundings, starts to vaporize. When the ignition criterion is reached, an envelope flame appears around the droplet, a luminous soot shell forms near the droplet, and a nonluminous flame zone appears outside the soot shell, as shown in Fig. 1. The following assumptions are made for reasons of simplicity: (1) gravity effect is ignored; (2) the droplet is spherical in shape; (3) the Dufour–Soret effect is negligible; (4) the liquid fuel is a gray body; (5) scattering effects are ignored in liquid radiative heat transfer; (6) the air is transparent to the radiative heat transfer; (7) the flame layer and soot shell are the two radiation sources and (8) the soot shell starts to emit radiant energy once the maximum gas-phase temperature reaches the flame temperature.

1. *Liquid phase* ($r < R_s$)

If the fuel droplet is considered as a semi-transparent material, the heat transfer inside of the droplet is given by

$$\nabla\cdot\left(\kappa r^2\frac{\partial T}{\partial r}-r^2 q_r\right)=\rho C_p\frac{\partial T}{\partial t}. \tag{1}$$

The radiation part of equation (1) is solved using the collocation method suggested by Tsai and Özişik [16]

$$\frac{1}{r^2}\frac{\partial r^2 q_r}{\partial r}=(1-\omega)[4n^2\sigma T^4-G(\tau)]. \tag{2}$$

here the optical thickness is defined as

$$\tau=\int_0^{R_s}\alpha_\lambda(r)\,dr \tag{3}$$

and $G(\tau)$ is the incident radiation defined as

$$G(\tau)=D(\tau)+\frac{1}{2\tau}\int_0^{\tau_0}\tau'[H(\tau')+\omega G(\tau')]\times[E_1(|\tau-\tau'|)-E_1(\tau+\tau')]\,d\tau' \tag{4}$$

where $E_1(x)$ is the exponential integral function, and

$$D(\tau)=4n^2\sigma\int_0^1\cosh(\tau\mu)\times\exp[-\sqrt{(\tau_0^2-\tau^2(1-\mu^2))}]\,d\mu \tag{5}$$

$$H(\tau)=(1-\omega)4n^2\sigma T^4(\tau). \tag{6}$$

The temperature gradient is set to be zero at the boundary condition of $r=0$ in accordance with the symmetric assumption.

2. *Gas phase* ($r > R_s$)

The governing equations of the gas phase are the same as those used by Char and Fan [17] and are described briefly below.

Continuity equation for species k:

$$\frac{\partial\rho_k}{\partial t}+\frac{1}{r^2}\frac{\partial}{r}(r^2\rho_k u)=\frac{1}{r^2}\frac{\partial}{r}\left(r^2\rho D\frac{\partial}{\partial r}Y_k\right)+\dot\rho_k^c. \tag{7}$$

Momentum equation for the gas phase mixture:

$$\frac{\partial}{\partial t}(\rho u)+\frac{1}{r^2}\frac{\partial}{\partial r}(r^2\rho u^2)=-\frac{\partial p}{\partial r}+\frac{1}{r^2}\frac{\partial}{r}(r^2\tau_{rr})-\frac{\tau_{\theta\theta}+\tau_{\phi\phi}}{r}. \tag{8}$$

Energy equation for the gas phase mixture:

$$\frac{\partial}{\partial t}(\rho I)+\frac{1}{r^2}\frac{\partial}{r}(r^2\rho u I)=-\frac{p}{r^2}\frac{\partial}{\partial r}(r^2u)+\frac{1}{r^2}\frac{\partial}{\partial r}\left(\kappa r^2\frac{\partial T}{\partial r}\right)+\frac{1}{r^2}\left\{\frac{\partial}{\partial r}\left[r^2\left(\sum_{k=1}^{N}h_k\frac{\partial Y_k}{\partial r}\right)\right]\right\}+\tau_{rr}\frac{\partial u}{\partial r}+(\tau_{\theta\theta}+\tau_{\phi\phi})\frac{u}{r}+\dot\omega Q \tag{9}$$

and

$$I=\sum_{k=1}^{N}Y_k I_k(T) \tag{10}$$

and the species specific enthalpy of ideal gas component is

$$h_k=I_k+\frac{p}{\rho_k}=I_k+\frac{R_u T}{W_k}. \tag{11}$$

The outmost boundary conditions ($r\to\infty$) are set to be the ambient conditions:

$$T = T_\infty \quad Y_F = 0 \quad Y_O = Y_{O,\infty} \quad p = p_\infty. \tag{12}$$

3. *The interface boundary conditions* ($r = R_s$)

Fuel mass fraction:

$$-\rho D \frac{\partial Y_F}{\partial r}|_{r=R_s} = \dot{m}[1-(Y_F)_s]. \tag{13}$$

Oxidizer mass fraction:

$$\rho D \frac{\partial Y_O}{\partial r}|_{r=R_s} = \dot{m}(Y_O)_s. \tag{14}$$

Energy:

$$\sigma\varepsilon_g F_{\lambda T_g \to \infty} T_g^4 + \sigma\varepsilon_s F_{\lambda T_s \to \infty} T_s^4 - \sigma\varepsilon_l F_{\lambda T \to \infty} T^4 + \kappa \frac{\partial T}{\partial r}|_{r=R_s} = \kappa_l \frac{\partial T_l}{\partial r}|_{r=R_s} + \dot{m}L. \tag{15}$$

Evaporation rate of fuel vapor:

$$\dot{m} = -\rho_l \frac{dR_s}{dt} = \rho\left(u - \frac{dR_s}{dt}\right). \tag{16}$$

Fuel vapor concentration at the surface can be obtained by use of the Clausius–Clapeyron equation:

$$(X_F)_s p = p_0 \exp\left[\frac{LW_F}{R_u}\left(\frac{1}{T_0} - \frac{1}{T_s}\right)\right]. \tag{17}$$

4. *Chemical reaction model*

One-step reaction equation:

$$\nu_F F + \nu_0 O \to \nu_p P. \tag{18}$$

Based upon the available data given by Westbrook and Dryer [18], the chemical reaction rate for equation (9) is expressed by

$$\dot{\omega} = C_f \exp(-E_a/T)\left(\frac{\rho_F}{W_F}\right)^{\alpha'_F}\left(\frac{\rho O}{W_O}\right)^{\alpha'_O}. \tag{19}$$

For benzene fuel: $\alpha'_F = -0.1$ and $\alpha'_O = 1.85$.

Flammability: lower bound $\phi_L = 0.5$ and upper bound $\phi_R = 3.6$.

The reaction rate coefficient and the activation energy will be determined later.

The variable thermophysical properties such as C_p, ν, D and κ are functions of temperature and are obtained from Vargaftik [19], Reid *et al.* [20] or Daubert and Danner [21].

5. *Radiative properties*

The liquid fuel transmission spectrum in the infrared range is obtained from the Sadtler handbook of infrared spectra by Simons [22], in which the data is measured transmission fraction vs wavelength. Friedman and Churchill [23] calculated the JP-4 fuel droplet radiation absorption coefficient from the transmission data by using the Bouguer–Beer law

$$\Gamma_{\lambda,x} = \exp(-\alpha_\lambda x). \tag{20}$$

The spectral absorption coefficient of liquid benzene calculated from equation (20) is shown in Fig. 2. At several wavelengths there are strong absorptive peaks which do absorb radiant energy in the infrared range. Thus, this identifies that liquid benzene fuel is not fully transparent to the radiation transfer.

Soot particles in droplet diffusion flames are generally small, as indicated by Abdel-Khalik *et al.* [24]. If the size is small compared to the wavelength, the Rayleigh limit is applicable for soot radiation calculations. Under this limit, the benzene flame soot spectral extinction coefficient is given by Tien and Lee [25]

$$k_{s\lambda} = \frac{36\pi n\kappa}{(n^2-\kappa^2+2)^2+4n^2\kappa^2} f_v \lambda^{-c} \tag{21}$$

where the value of the complex refractive index $n+i\kappa$, measured by Erickson *et al.* [26], is $1.6–0.6i$, and the power c of wavelength of soot for benzene flame can be obtained as a function of the wavelength from the experimental data of Siddall and McGrath [27]. Thus, the spectral emissivity from Tien and Lee [25] is expressed as

$$\varepsilon_{s\lambda} = 1 - e^{k_{s\lambda} x_s}. \tag{22}$$

Spectral emissivity is shown as the dashed line in Fig. 2, restricted in that the experimental data were only measured within limited narrow bands ($\leqslant 6$ μm wavelength). Berlad and Hibbard [28] argued that gaseous radiation bands do not generally coincide with the absorption bands of most liquid fuels; but in comparing the absorption coefficient curve of liquid benzene and the emissivity curve of soots in Fig. 2, it is apparent that some absorption peaks of liquid benzene occur in the soot emission spectrum. Therefore, the absorption of radiation energy by liquid fuel can be verified. Faeth [2] also concluded that radiation is more important when there is significant continuum radiation from hot surfaces and soot.

All radiative properties are spectral, but the gray body assumption, that properties are independent of wavelength, simplifies the computation efforts. For a semitransparent fuel, the Planck mean absorption coefficient α_p is given by Özişik [29]

$$\alpha_p = \sum_{m=1}^{M} \alpha_m [F_{0-\lambda_m}(T) - F_{0-\lambda_{m-1}}(T)]. \tag{23}$$

The calculated mean absorption coefficient which varies with temperature is shown in Fig. 3. The results indicate that an increase in the temperature of radiation source decreases the value of the coefficient, thus the optical thickness of the liquid fuel decreases when there is a relatively high temperature emission source. It means that liquid benzene becomes rather transparent to radiation in a higher temperature environment.

Nonluminous flame emissions are mainly due to water vapor and carbon dioxide of the combustion products. The semi-empirical relation of gas emissivity expressed by Taylor and Foster [30] is

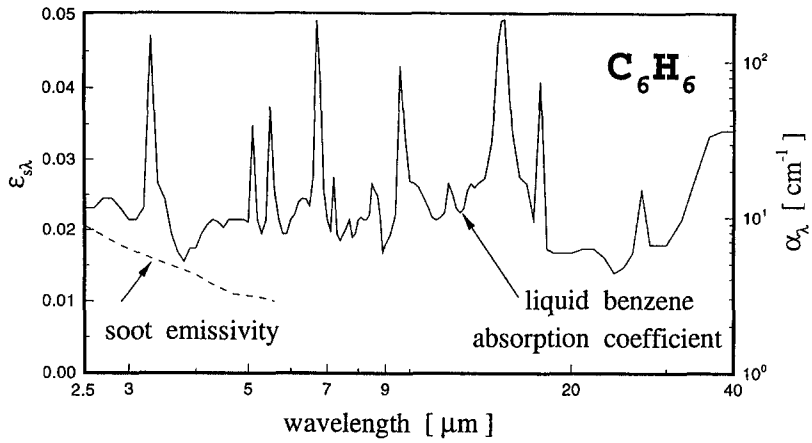

Fig. 2. Spectral absorption coefficient of liquid benzene and soot emissivity in infrared range.

$$\varepsilon_g = \sum_{i=1}^{4} (b_{1,i} + b_{2,i} T)(1 - e^{-\alpha_{g,i}(p_c + p_w)x}) \quad (24)$$

while the luminous flame emissivity of the soot shell as established by Felske and Tien [31] is

$$\varepsilon_s = 1 - \frac{15}{\pi^4} \psi^{(3)}\left(1 + \frac{c f_v x_s T}{C_2}\right) \quad (25)$$

where $\psi^{(3)}$ is the pentagamma function (see Abramowitz and Stegun [32]).

NUMERICAL METHOD

The gas-phase governing equations are in the form of partial differential equations with convection and diffusion terms. To deal with such equations, the power-law scheme [33] is applied to discretize equations (7)–(9). Both gas- and liquid-phases governing equations are solved using the finite-volume method [33]. The coupling between velocity and pressure is treated with the SIMPLER algorithm [33]. The solution procedure is described below:

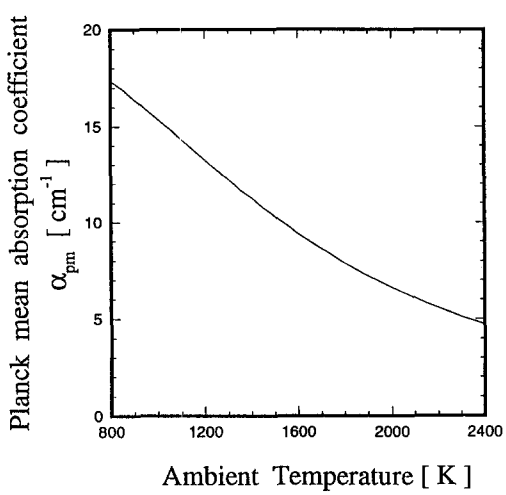

Fig. 3. Planck mean absorption coefficient of liquid benzene vs ambient temperature.

(1) Guess an evaporation rate $\dot{m}$ and use the data of the previous time step for other thermochemical properties required at the first iteration.

(2) Find the mass fractions Y_F and Y_O from equations (13) and (14).

(3) Use the Clausius–Clapeyron equation (17) to obtain the surface temperature T_s.

(4) Solve the gas-phase governing equations (7)–(9).

(5) Solve the liquid-phase governing equations (1).

(6) Substitute the up-to-date data into the interface energy equation (15) to find a new evaporation rate $\dot{m}$.

(7) If the convergent criterion is met, move to the next time step; otherwise, go back to step (2) and repeat the calculation procedure until $\dot{m}$ is converged. The convergence criterion is set as

$$\left|\frac{\dot{m}^{n+1} - \dot{m}^n}{\dot{m}^n}\right| < 10^{-4}.$$

In order to achieve a better resolution in the high-temperature-gradient regions, the adaptive grid generation method developed by Dwyer *et al.* [34] is utilized here to optimize the grid distribution in the gas phase. With this grid generation method, the grid increment becomes smaller in the regions where the rate of temperature change is larger.

RESULTS AND DISCUSSION

In simulating the droplet combustion process under the conditions with simple one-step chemical reaction model, reaction rate constants are crucial parameters. The constants given by Westbrook and Dryer [18] are only suitable at low temperatures and for large scale premixed flames, as indicated by Bergeron and Hallett [4], who also extracted reaction rate constants from their droplet ignition experiments. The radiation effect was considered in their modeling. Bergeron and Hallett [4], however, provided insufficient data in regard to a radiative source used in their model prior to

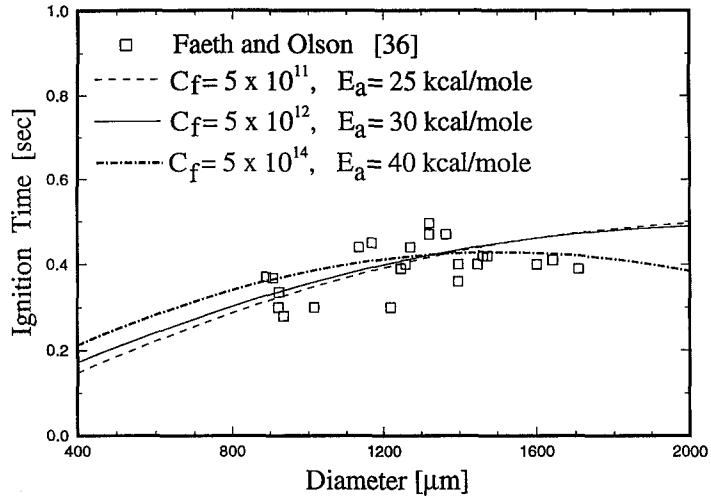

Fig. 4. Sensitivity study of reaction rate coefficient and activation energy.

ignition of the droplets. Thus, their data is unsuitable to use in simulating present droplet combustion without any radiation source prior to ignition (see the assumption (7)). Shieh and Chang [35] applied the reaction rate constants suggested by Bergeron and Hallett [4] to simulate *n*-heptane droplet combustion, but the ignition delay times did not agree with the measured data [4] especially in the low ambient temperature condition. Therefore, sensitivity of reaction rate constants were studied by comparing the ignition times of Faeth and Olson [36], whose experiments were conducted under microgravity conditions to guarantee droplet spherical symmetry. The reaction rate coefficient C_f and activation energy E_a were the two parameters examined in the sensitivity study, while the other constants provided by Westbrook and Dryer [18] remained the same. Westbrook and Dryer [18] argued that the effective activation energy falls between the lower value ($\approx$26 kcal mol^{-1}) and the higher value (40 kcal mol^{-1}). Because Westbrook and Dryer [18] used an appropriate average value of 30 kcal mol^{-1}, three activation energy values, 25, 30 and 40 kcal mol^{-1}, were chosen in this study, and many different values of C_f were tried to suit the measured ignition time data. The optimal values of C_f for different E_a are shown in Fig. 4.

Another group of ignition time data (Bergeron and Hallett [4], Kobayasi [10]) was produced at different ambient temperatures for the same size droplets. Figure 5 shows three groups of data. Only that by Faeth and Olson [36] was done under microgravity conditions. Because all the measured data were taken within the size range of 1200 and 1500 μm, two cases with initial droplet diameters of 1200 and 1500 μm were tested here. Three different sets of C_f and E_a shown in Fig. 4 were examined. Comparative results with the experimental data revealed that the set with $C_f = 5 \times 10^{14}$ and $E_a = 40$ kcal mol^{-1} led to the most satisfactory agreement, as shown in Fig. 5. The results were good for the data of Faeth and Olson [36] at a relatively high surrounding temperature, and good for data of Bergeron and Hallett [4] at a lower temperature. Kobayasi [10] investigated two cases of different droplet sizes at a medium temperature of 1013 K. The results were good for his data. Therefore, the remaining study will use $C_f = 5 \times 10^{14}$ and $E_a = 40$ kcal mol^{-1} for droplet combustion simulation.

Three different conditional cases were investigated in this work: Case 1, without radiation heat transfer; Case 2, opaque droplet with flame emission and Case 3, semitransparent droplet with flame emission. Large amounts of information about single droplet combustion experiments can be found over recent years, but most experiments were conducted under the condition of forced ignition, for instance, Hara and Kumagai [13] and Jackson and Avedisian [37]. Thus the diameter square data provided by these experiments are only for the post-ignition period. Moreover, lack of the completely measured initial condition right after ignition may introduce significant prediction uncertainty in model simulation. The experiments of Kobayasi [10] provided complete data from the stages of heating, to evaporation, to ignition, to combustion, to droplet vanishing. Because his experiment was conducted under normal gravity environment, the reported data of the diameter square of droplet was corrected from an ellipsoid to an equivalent sphere [10]. The three different cases were run under the same test conditions as those of experiment [10], except the buoyancy effects were neglected in the work.

When ignition occurs, the peak temperature of the gas phase jumps up suddenly. Based upon this observation, the ignition delay time can be defined as the inflection point in the plot of peak temperature vs time, i.e.

$$\frac{d^2 T_{max}}{dt^2} = 0. \tag{26}$$

This criterion has been used in most of the theoretical

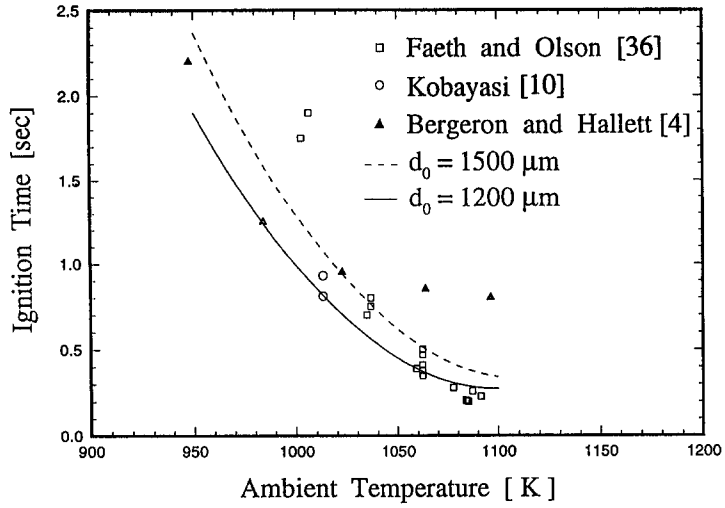

Fig. 5. Calculated and measured ignition delay times for benzene droplets.

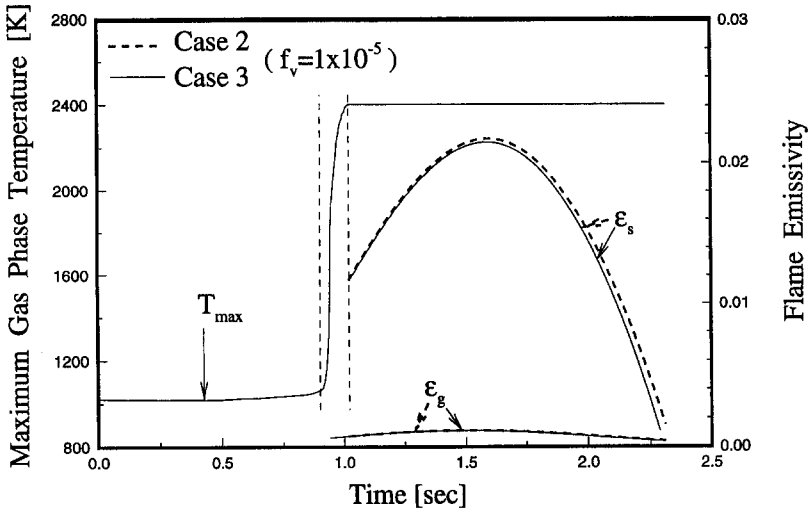

Fig. 6. Maximum gas phase temperature and flame emissivity vs time for Cases 2 and 3.

models, including those of Rah *et al.* [38], Char and Fan [17] and Niioka *et al.* [39]. The maximum gas phase temperature variation in time is shown in Fig. 6. It is clear that the inflection point is about 1700 K in our studies. The determination of ignition occurring in experimental observation is easy to make when the first visible flame appears, but the theoretical analysis of ignition phenomena cannot be precisely determined by this simple mathematical formula. Thus, the time interval within the dashed-line region on Fig. 6 indicates the instant that ignition could happen. Figure 6 also demonstrates the emissivities of luminous and nonluminous flames for Cases 2 and 3. Obviously, luminous soot emission is much stronger than the nonluminous emissions of carbon dioxide and water vapor, which is consistent with the viewpoint of Siegel and Howell [8]. The values of ε_s and ε_g vary with the flame radius (see Figs. 6 and 7), because equations (24) and (25) relate to flame size and soot layer thickness. Gaseous emission is almost the same in both cases (cf. Fig. 6), so the influence of the combustion products on gaseous radiation is small in droplet combustion. According to the experimental observations of Hara and Kumagai [13], the ratios of flame radius to soot radius (R_f/R_s) in the burning process were maintained between 4 and 5 in the burning process. The experimental study of Jackson and Avedisian also revealed that this ratio was not constant but rather time dependent. A sensitivity study revealed that the influences of R_f/R_s values changing from 4 to 5 on the determination of ε_s were less significant than those of f_v values changing from 10^{-7} to 10^{-5}, as displayed in Fig. 8. Lacking the exact relation between this ratio with time, this value is thus set to be 4 in the present

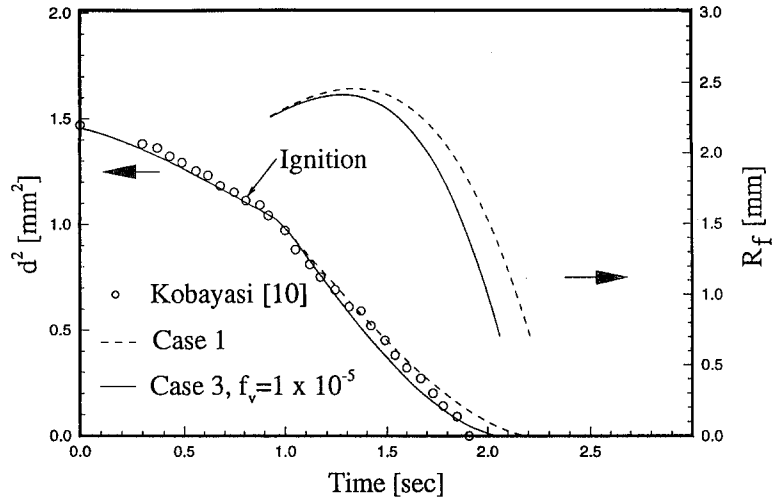

Fig. 7. Comparisons of diameter square and flame radius for Cases 1 and 3 with the measured data (d_0 = 1.212 mm).

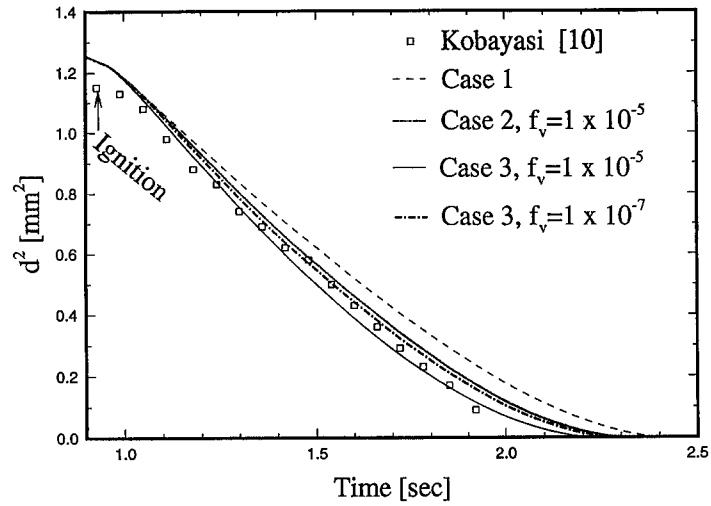

Fig. 8. Comparisons of diameter square in the burning period for three cases (d_0 = 1.277 mm).

study. In addition, the sooty layer did not appear immediately at the time of ignition in their experimental observation [13, 37], but there is no exact data on this delay. In our model, it is assumed that the luminous flame starts to emit radiant energy once the maximum gas phase temperature rises to meet the flame temperature ($\approx$2400 K, see Fig. 6).

The soot volume fraction has different ranges reported in the literature, 7.0×10^{-8}–1.0×10^{-7} [24], 10^{-7}–10^{-5} [40] and 10^{-8}–10^{-6} [8]. The values of 10^{-7} and 10^{-5} are examined here, and their effects on the diameter square are displayed in Fig. 8. It is seen that the choice of f_v values between 10^{-7} and 10^{-5} certainly affects the predicted curve of d^2 but their effects are less than those between Cases 2 and 3. The soot emission in the case of opaque droplets is slightly larger than that in semitransparent droplets in the final period of burning (cf. Fig. 6). That is because the regression rate of Case 2 is slower than that of Case 3, while the calculated flame thicknesses of both cases are nearly the same.

The experiments of Kobayasi [10] provide the diameter square of a benzene droplet through the whole burning process, thus the measured data are a valid comparative reference for the theoretical results. Figures 7 and 9 are the d^2 predictions compared to the experiments with initial diameters of 1212 and 1277 μm, respectively. The results show that our predictions on the evaporation process agree with the data in Fig. 7, but deviate relatively significantly from Fig. 9. The criterion $d^2\ T_{max}/dt^2 = 0$ to determine the ignition delay time was used in the present theoretical analysis. But it should be noted that ignition may happen at any instant that the maximum gas phase temperature begins to increase from the ambient temperature to the flame temperature. This time interval is about 0.1 s (see Fig. 6). Therefore, the predicted ignition delays could deviate from the measured data in this range.

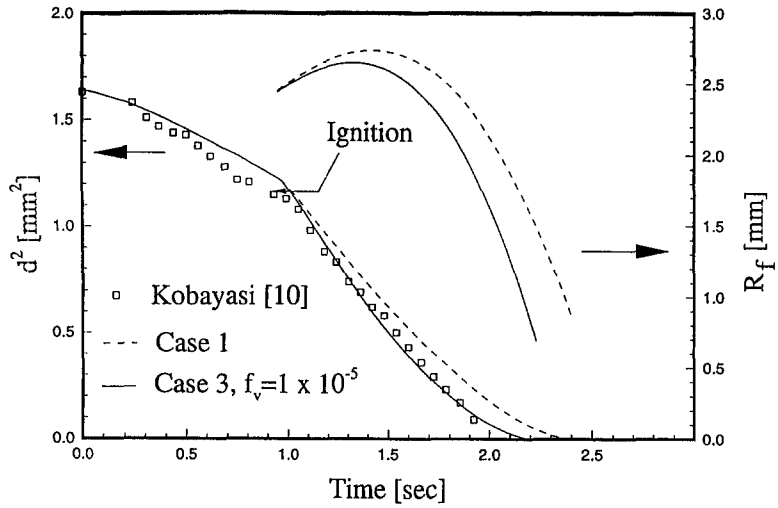

Fig. 9. Comparisons of diameter square and flame radius for Cases 1 and 3 with the measured data (d_0 = 1.277 mm).

Predictions on the burning period for Case 3 are in comparatively good agreement with the measured data, shown in Figs. 7 and 9, as compared to those for Case 1. The regression rate of Case 1 is slower than that of Case 3. That is reasonable, because Case 1 excludes all radiative effects. These two figures also show the flame radius for both cases, with the flame size slightly increasing and then shrinking back to the droplet sides.

For a detailed comparison of the three cases, the burning d^2 with d_0 = 1277 μm is magnified in Fig. 8. It is clear that the measured data is rather close to Case 3 regardless of the amount of soot concentration (f_v is between 10^{-7} and 10^{-5}). Opaque droplets (Case 2) burn slightly slower than Case 3 (for both f_v values).

In the previously mentioned results, the plots of the d^2 curve did not follow straight lines, especially in the final burning period for any case with or without considering the effects of radiation. The classical d^2 law is based on the following assumptions: (1) constant properties; (2) a uniform droplet temperature; (3) an unchanging standoff ratio (flame-to-droplet radii) and (4) flame extinction at the instant that the liquid droplet vanishes. However, these conditions did not exist in our study. Therefore, the d^2 law is not valid for use in most real droplet combustion processes. This conclusion has been corroborated by several studies through experimental observation and theoretical analysis [41–43].

Droplet temperature distribution variations in time for Cases 1 and 3 are shown in Figs. 10–12, and the conduction and radiation heat fluxes are represented by the vertical bars. The temperatures and conduction heat flux q_c at the pre-ignition stage is shown in Fig. 10 for four time steps. Note that there is no radiant heat source outside the droplet before the flame is formed. In the present study, a fuel droplet with an initial temperature of 300 K entering a hot air environment with 1013 K temperature leads to significant conduction heat flux near the droplet surface at the beginning stage. Since the droplet temperatures are bounded with the boiling point of benzene, the peak of q_c gradually moves toward the interior of the droplet as its surface temperature is close to the boiling point. Figure 11 shows the results at the post-ignition period of Case 1. Right after the ignition, the surrounding temperatures are increased very soon due to the exothermic effects of combustion reaction. As a result, the sudden increment of temperature gap at the interface, at the beginning time of the post-ignition period, leads to high q_c once more. For a totally trans-

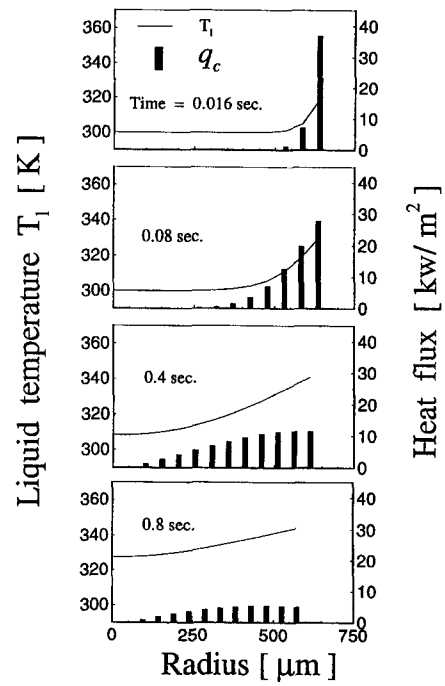

Fig. 10. Liquid phase temperatures and conduction heat fluxes at different time steps before ignition.

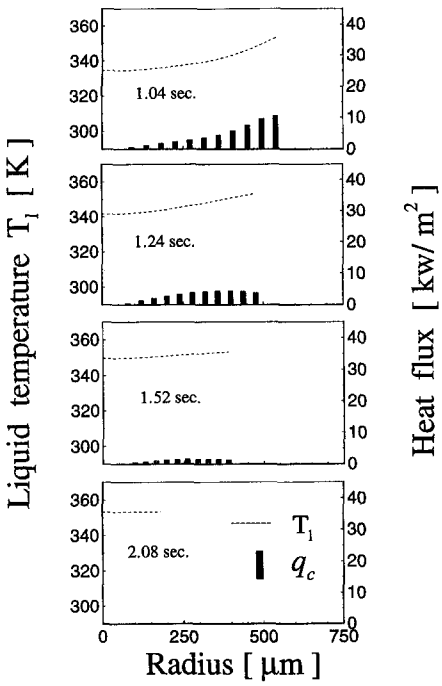

Fig. 11. Liquid phase temperatures and conduction heat fluxes at different time steps for Case 1 after ignition.

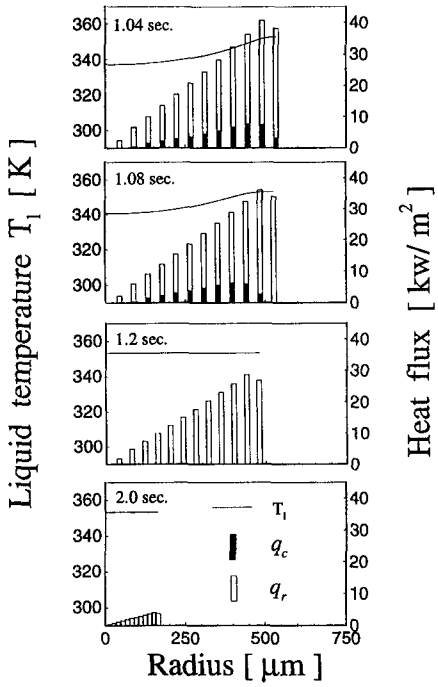

Fig. 12. Liquid phase temperatures and conduction heat fluxes at different time steps for Case 3 after ignition.

parent droplet, the temperature distribution becomes nearly uniform at 1.52 s. Only the thermal conduction transfer governs the energy transport in Case 1, so there is no heat transfer after the temperature levels off; but if radiative absorption is taken into account (Case 3), as shown in Fig. 12, there is considerable radiative heat flux even if there is a small temperature gradient or even when a whole droplet reaches the boiling point. Because of this, the temperature distribution inside the droplet becomes uniform earlier than the transparent case (Case 1). Based upon the definition of the optical thickness, equation (3), τ is the function of the droplet radius (R_s) and τ becomes smaller as R_s decreases. In other words, the droplet becomes more transparent as its size is reduced. This explains the less radiant heat flux absorbed by the droplet in the final period of burning process.

CONCLUSIONS

Single droplet combustion processes including heating, evaporation, ignition, burning and droplet vanishing are theoretically investigated by taking into account the flame radiation effect and radiant energy absorbed by liquid fuel. Benzene fuel droplets are tested in the numerical analysis and their predictions are compared with the available experimental data found in the literature. The following concluding remarks are then drawn from this study.

(1) The consideration of flame radiation on droplet combustion in the post ignition period leads to some differences in the prediction of the droplet regression rate. The prediction of the diameter square when flame radiation is considered agrees more with the experimental data than the case without flame radiation.

(2) The prediction for the opaque droplet burning rate is slower than that for the semitransparent case. That is because radiant energy does not penetrate into the liquid droplet and is only absorbed on the droplet surface. But the radiative absorption of liquid benzene is found, at least, in the infrared range. As a result, the liquid benzene is neither perfectly transparent nor opaque to thermal radiation, and the radiation absorbed by the benzene droplet cannot be ignored.

(3) Luminous flame emission is much larger (about ten times) than nonluminous flame emission. Therefore, the soot shell is the major contribution of flame radiation during the droplet burning process. The present study adopted the information of soot-layer thickness and soot volume fraction in the modeling work directly from the available experimental results. However, in order to construct a more comprehensive model, the determination of soot formation should be considered in the future formulation.

REFERENCES

1. C. K. Law, Recent advances in droplet vaporization and combustion, *Prog. Energy Combust. Sci.* **8,** 171–201 (1982).
2. G. M. Faeth, Evaporation and combustion of sprays, *Prog. Energy Combust. Sci.* **9,** 1–76 (1983).
3. R. Viskanta and M. P. Mengüç, Radiation heat transfer in combustion systems, *Prog. Energy Combust. Sci.* **13,** 97–160 (1987).
4. C. A. Bergeron and W. L. H. Hallett, Ignition characteristics of liquid hydrocarbon fuels as single droplets, *Can. J. Chem. Engng* **67,** 142–149 (1989).

5. T. Saitoh, K. Yamazaki and R. Viskanta, Effect of thermal radiation on transient combustion of a fuel droplet, *J. Thermophys. Heat Transfer* **7**, 94–100 (1993).
6. P. L. C. Lage and R. H. Rangel, Total thermal radiation absorption by a single spherical droplet, *J. Thermophys. Heat Transfer* **7**, 101–109 (1993).
7. P. L. C. Lage and R. H. Rangel, Single droplet vaporization including thermal radiation absorption, *J. Thermophys. Heat Transfer* **7**, 502–509 (1993).
8. R. Siegel and J. R. Howell, *Thermal Radiation Heat Transfer* (2nd Edn), Chap. 17. Hemisphere, New York (1981).
9. A. Sjögren, Soot formation by combustion of an atomized liquid fuel, *Proceedings of the Fourteenth International Symposium on Combustion*, pp. 919–927. The Combustion Institute, Pittsburgh (1973).
10. K. Kobayasi, An experimental study on the combustion of a fuel droplet, *Proceedings of the Fifth International Symposium on Combustion*, pp. 141–148. The Combustion Institute, Pittsburgh (1955).
11. J. A. Bolt and M. A. Saad, Combustion rates of freely falling fuel drops in a hot atmosphere, *Proceedings of the Sixth International Symposium on Combustion*, pp. 717–725. The Combustion Institute, Pittsburgh (1957).
12. A. L. Randolph and C. K. Law, Influence of physical mechanisms on soot formation and destruction in droplet burning, *Combust. Flame* **64**, 267–284 (1986).
13. H. Hara and S. Kumagai, Experimental investigation of free droplet combustion under microgravity, *Proceedings of the Twenty third International Symposium on Combustion*, pp. 1065–1611. The Combustion Institute, Pittsburgh (1990).
14. G. S. Jackson and C. T. Avedisian, Soot formation during combustion of unsupported methanol/toluene mixture droplets in microgravity, *Proc. R. Soc. Lond.* **A435**, 359–369 (1991).
15. G. S. Jackson, C. T. Avedisian and J. C. Yang, Observations of soot during droplet combustion at low gravity: heptane and heptane/monochloroalkane mixtures, *Int. J. Heat Mass Transfer* **35**, 2017–2033 (1992).
16. J. R. Tsai and M. M. Özişic, Transient, combined conduction and radiation in an absorbing, emitting, and isotropically scattering solid sphere, *J. Quant. Spectrosc. Radiat. Transfer* **38**, 243–251 (1987).
17. J. R. Char and M. Y. Fan, The parametric study of ignition process of a fuel droplet, *Int. J. Turbo Jet Engines* **10**, 83–96 (1993).
18. C. Westbrook and F. Dryer, Simplified reaction mechanism for the oxidation of hydrocarbon fuels in flames, *Combust. Sci. Technol.* **27**, 31–43 (1981).
19. N. B. Vargaftik, *Tables on the Thermophysical Properties of Liquids and Gases* (2nd Edn), pp. 342–346. Hemisphere, Washington (1975).
20. R. C. Reid, J. M. Prausnitz and B. E. Poling, *The Properties of Gases and Liquids* (4th Edn), pp. 388–631. McGraw-Hill, New York (1987).
21. T. E. Daubert and R. P. Danner, *Physical and Thermodynamic Properties of Pure Chemicals: Data Compilation* (1st Edn). Hemisphere, New York (1989).
22. W. W. Simons, *The Sadtler Handbook of Infrared Spectra* (1st Edn), p. 59. Sadtler Research Laboratories, Philadelphia (1978).
23. M. H. Friedman and S. W. Churchill, The absorption of thermal radiation by fuel droplets, *Chem. Engng Prog. Symp. Ser.* **61**, 1–4 (1965).
24. S. I. Abdel-Khalik, T. Tamaru and M. M. El-Wakil, A chromatographic and interferometric study of the diffusion flame around a simulated fuel drop, *Proceedings of the Fifteenth Internal Symposium on Combustion*, pp. 389–399. The Combustion Institute, Pittsburgh (1974).
25. C. L. Tien and S. C. Lee, Flame radiation, *Prog. Energy Combust. Sci.* **8**, 41–59 (1982).
26. W. D. Erickson, G. C. Williams and H. C. Hottel, Light scattering measurements on soot in a benzene–air flame, *Combust. Flame* **8**, 127–132 (1964).
27. R. G. Siddall and I. A. McGrath, The emissivity of luminous flames, *Proceedings of the Ninth International Symposium on Combustion*, pp. 102–110. The Combustion Institute, Pittsburgh (1964).
28. A. Berlad and R. Hibbard, Effect of radiant energy on vaporization and combustion of liquid fuels, NACA RME-52109 (1952).
29. M. M. Özişic, *Radiative Transfer and Interactions with Conduction and Convection* (1st Edn), p. 25. John Wiley, New York (1973).
30. P. B. Taylor and P. J. Foster, The total emissivities of luminous and nonluminous flames, *Int. J. Heat Mass Transfer* **17**, 1591–1605 (1974).
31. J. D. Felske and C. L. Tien, Calculation of the emissivity of luminous flames, *Combust. Sci. Technol.* **7**, 25–31 (1973).
32. M. Abramowitz and I. A. Stegun, *Handbook of Mathematical Functions* (9th Edn), pp. 260. U.S. Government Printing Office, Washington (1970).
33. S. V. Patankar, *Numerical Heat Transfer and Fluid Flow* (1st Edn), Chaps 5 and 6. Hemisphere, New York (1980).
34. H. A. Dwyer, B. R. Sanders and F. Raiszadek, Ignition and flame propagation studies with adaptive numerical grids, *Combust. Flame* **52**, 11–23 (1983).
35. J. S. Shieh and K. C. Chang, Re-examination of droplet combustion process by considering thermal radiative transfer, *Proceedings of the Fifth Australasian Heat and Mass Transfer Conference*, pp. (24-) 1–6. The University of Queensland, Brisbane (1993).
36. G. M. Faeth and D. R. Olson, The ignition of hydrocarbon fuel droplets in air, *SAE Trans.* **77**, 1793–1802 (1968).
37. G. S. Jackson and C. T. Avedisian, The effect of initial diameter in spherically symmetric droplet combustion of sooting fuels, *Proc. R. Soc. Lond.* **A446**, 255–276 (1994).
38. S.-C. Rah, A. F. Sarofim and J. M. Beèr, Ignition and combustion of liquid fuel droplets—II. Ignition studies, *Combust. Sci. Technol.* **49**, 169–184 (1986).
39. T. Niioka, S. Ishiguro and T. Saitoh, A numerical approach to fuel droplet ignition, TR-628T, National Aerospace Laboratory, Tokyo (1980).
40. K. Y. Lee, Z. Y. Zhong and C. L. Tien, Blockage of thermal radiation by the soot layer in combustion of condensed fuels, *Proceedings of the Twentieth International Symposium on Combustion*, pp. 1629–1636. The Combustion Institute, Pittsburgh (1984).
41. H. Krier and J. A. Wronkiewicz, Combustion of single drops of fuel, *Combust. Flame* **18**, 159–166 (1972).
42. C. H. Waldman, Theory of non-steady state droplet combustion, *Proceedings of the fifteenth International Symposium on Combustion*, pp. 429–442. The Combustion Institute, Pittsburgh (1975).
43. C. K. Law and G. M. Faeth, Opportunities and challenges of combustion in microgravity, *Prog. Energy Combust. Sci.* **20**, 65–113 (1994).